Resolution Enhancement and Interference Suppression for Planetary Radar Sounders

Maria Carmela Raguso[A,C], Lorenzo Piazzo[A], Marco Mastrogiuseppe[A], Roberto Seu[A], Roberto Orosei[B]

(A) DIET Dept., Sapienza University, Rome, Italy   (B) IAPS Inst., Istituto Nazionale di Astrofisica, Rome, Italy

(C) Corresponding author. Email: raguso@diet.uniroma1.it

Abstract— **Orbital radar sounders are an effective tool to investigate the interior of planetary bodies. Typically, the sounding signal lies in the High Frequency (HF) or Very High Frequency (VHF) band, allowing a good ground penetration but a limited range resolution. Moreover, Electromagnetic Interference (EMI) may affect the system, increasing the noise in the radar products. In this paper, we propose methods to enhance the resolution and to suppress the EMI, exploiting a linear prediction based approach. Using simulated data, we investigate the methods' performance and the parameter settings. Finally, we apply the methods to data of the Mars Advanced Radar for Subsurface and Ionosphere Sounding (MARSIS).**

I. INTRODUCTION

Radar sounding is an attractive technique for exploring the interior of planetary bodies, allowing the investigation of the subsurface structures. Radars with sounding capabilities have been included in the payload of several missions, like the Apollo Lunar Sounder Experiment (ALSE) on board the Apollo Mission [1], the Mars Advanced Radar for Subsurface and Ionosphere Sounding (MARSIS) on board the European Space Agencys (ESA) orbiter Mars Express [2], the Shallow Radar (SHARAD) mounted on the National Aeronautics and Space Administrations (NASA) orbiter Mars Reconnaissance Orbiter (MRO) [3] and the Lunar Radar Sounder of the Japanese orbiter Kayuga [4]. Radar sounders are also included in the payload of future missions, like the Radar for Icy Moons Exploration (RIME) [5] and the Europa CLIPPER mission [6].

In order to perform subsurface investigation, radar sounders usually exploit wideband signals in the High-Frequency (HF) or Very High-Frequency (VHF) bands. These bands are vulnerable to electromagnetic interferences (EMI) which can reduce the sensitivity of the instrument and the quality of radar products. Furthermore, the instruments operating at HF have a limited resolution, since the latter is dictated by the signal bandwidth which, in turn, is limited by the need to keep low the fractional bandwidth.

In this paper we tackle the above mentioned problems and discuss methods to suppress the EMI and to increase the range resolution. The methods are based on extrapolation and interpolation of the signal spectrum, accomplished by means of linear prediction techniques. This approach is not new and has been exploited earlier. Indeed, a seminal work is [7], where bandwidth extrapolation (BWE) was proposed in order to improve the resolution of an imaging radar. Later, the BWE was applied to wideband radars [8]. Moreover, in [9] linear prediction is exploited in order to improve the resolution of a

Synthetic Aperture Radar (SAR). Finally, similar techniques have been successfully applied to the Cassini Radar [10]. However, to the best of our knowledge, this technique has never been applied to radar sounders neither to the EMI suppression problem. As an additional contribution, we discuss a specific example, illustrating the application of the methods to the MARSIS data. In a companion paper, the application to SHARAD data has been considered [11]. Moreover, an alternative super-resolution approach for MARSIS is presented in [12].

The paper is organized as follows. In Section II we describe the radar sounder model. In Section III we briefly review linear prediction. In Section IV we present the resolution enhancement and the EMI suppression methods. In Section V we discuss the application to MARSIS data and in Section VI we give the conclusions.

II. RADAR SOUNDING

A planetary radar sounder is a HF or VHF radar onboard a spacecraft orbiting the planet. The sounder transmits a sequence of pulses (chirps) towards the planet. When a pulse hits a medium discontinuity, it is partially reflected and refracted. Some energy passes the discontinuity and is reflected and refracted by successive discontinuities. The sounder receives the reflected pulses and, by means of proper processing, reconstructs the layer structure of the explored area.

After transmitting a chirp $p(t)$, having bandwidth B centered on a carrier frequency f_c, the sounder switches to the receive mode and collects the return signal for a time T_f, which is assumed to be sufficient to collect all the echoes of interest. This signal is sampled and fed to a filter matched to the chirp, usually realized in the frequency domain. This processing is known as pulse compression because every copy of $p(t)$ entering the filter is transformed into a shorter, compressed pulse, which is ideally sinc shaped, with a -4 dB main lobe having a duration $T = 1/B$. In turn, the main lobe sets the instrument's range resolution, which is inversely proportional to the chirp bandwidth.

The signal at the output of the matched filter is called a *data frame*. The data frames corresponding to the various transmitted pulses are stacked into an array which is known as a radargram, yielding information about the layer structure for a wide swath of terrain. Typically the frame is weighted in the frequency domain with a proper window (e.g. Hamming, Hanning, Bartlet) in order to reduce the side-lobes of the
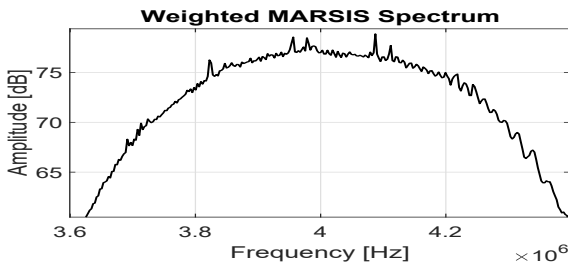
Fig. 1. A Hanning weighted MARSIS spectrum: the EMI peaks are clearly visible.

compressed pulse at the expense of a widening of the main lobe. Moreover, Doppler processing can be applied to the radargram in order to reduce the clutter [13].

The received signal is affected by noise due to several sources. First, there is additive noise due to the readout electronics and to the galactic noise. This noise can be modeled as a zero-mean, white stochastic process, with Gaussian distribution. A second noise source is the electro-magnetic interference (EMI) due to the coupling of the antenna with other subsystems of the instrument, like the solar panel, the clocks and so on. The EMI can be modeled as a set of sinusoidal signals superimposed to the received signal. In the signal spectrum, the EMI can be seen as a set of sharp peaks, centered at the sinusoids frequencies, see Figure 1.

It is convenient to introduce a simplified[1] model for the low-pass equivalent compressed signal. Specifically, the signal, for $|t| < \frac{T_f}{2}$, can be written as

$$r(t) = \sum_{i=1}^{L} \alpha_i \mathrm{sinc}\left(\frac{t - \tau_i}{T}\right) + \sum_{i=1}^{I} \beta_i e^{2\pi f_i t} \mathrm{rect}\left(\frac{t}{T_f}\right) + n(t) \tag{1}$$

where L is the number of layers, α_i and τ_i are the complex amplitude and the delay of the return pulse from the i-th layer, I is the number of EMI signals, β_i and f_i are the complex amplitude and frequency of the i-th EMI and $n(t)$ is white noise, with variance σ_n^2. Moreover, we define a Signal to Noise Ratio (SNR) as the return power from the strongest layer (which is typically the surface) to the noise variance, namely $SNR = max_i(|a_i|^2)/\sigma_n^2$. Finally, by taking the Fourier Transform (FT) of the latter expression and by neglecting some border effects, we obtain an expression for the spectrum of the compressed frame which, for $|f| < \frac{B}{2}$, is

$$R(f) = \sum_{i=1}^{L} \alpha_i e^{2\pi \tau_i f} \mathrm{rect}\left(\frac{f}{B}\right) + \sum_{i=1}^{I} \beta_i \mathrm{sinc}\left(\frac{f - f_i}{B_f}\right) + N(f) \tag{2}$$

where $B_f = 1/T_f$ is the inverse of the frame duration.

III. LINEAR PREDICTION

Given an N samples data sequence $x[i]$ for $i = 1, ..., N$, linear prediction considers the problem of approximating

[1] A realistic model shall include additional effects, like inter-layer reflections, clutter and non flat noise.

a sample as a linear combination the preceding (past) M samples. The coefficients to be used in the combination are denoted by a_k for $k = 1, ..., M$ and are called the (forward) prediction coefficients. In order to determine a suitable set of prediction coefficients, we first write the linear combination explicitly as

$$x^f[i] = \sum_{k=1}^{M} a_k x[i - k] \quad i = M + 1, ..., N \tag{3}$$

where $x^f[i]$ is the (forward) predicted sequence, representing the approximation of the i-th sample obtained by combining the preceding M samples. Next, we introduce the prediction error (for $i = M + 1, ..., N$), given by

$$e^f[i] = x[i] - x^f[i] = x[i] - \sum_{k=1}^{M} a_k x[i - k],$$

representing the difference between the predicted and the actual values. Finally, the coefficients are computed by minimizing the error energy, given by

$$E^f = \sum_{i=M+1}^{N} |e^f[i]|^2,$$

which involves the solution of a linear system [14]. The latter way of computing the coefficients is known as the Covariance (COV) method.

Once the coefficients have been computed, they can be used to predict future samples of the sequence, by using Equation (3) with $i > N$. However, for $i > N + 1$ the right hand side of the Equation cannot be computed, because it involves samples of $x[i]$ for $i > N$, which are not known. This problem is circumvented by using $x^f[i]$ instead of $x[i]$ for $i > N$, i.e. by using the predicted samples instead of the original samples. In this way, the predicted sequence $x^f[i]$ becomes the output of an Auto-Regressive (AR) filter and can be produced up to any desired length.

An entirely similar approach can be used in order to predict a sample as a linear combination the following (future) M samples, which is known as a backward prediction. In particular, we write the backward predicted sequence as

$$x^b[i] = \sum_{k=1}^{M} b_k x[i + k] \quad i = 1, ..., N - M$$

where b_k for $k = 1, ..., M$ are the backward prediction coefficients. Next, we introduce a backward prediction error (for $i = 1, ..., N - M$), given by

$$e^b[i] = x[i] - x^b[i] = x[i] - \sum_{k=1}^{M} b_k x[i + k].$$

Finally, the coefficients are computed by minimizing the error energy, given by

$$E^b = \sum_{i=1}^{N-M} |e^b[i]|^2.$$

Interestingly, when the data sequence is the sum of L complex sinusoidal signals, it can be exactly predicted, either backward or forward, using $M = 2L$ coefficients. This is because a sample of a sinusoidal signal can be exactly obtained as the linear combination of two past or future samples, see [14]. Moreover, the backward coefficients are simply the complex conjugate of the forward ones, i.e. $b_i = a_i^*$. The latter facts are important for our development. Indeed, Equation 2 shows that the received spectrum is a sum of sinusoidal signals plus EMI and noise. Due to the presence of the noise, we cannot achieve a perfect prediction. However, when the SNR is high, we expect the prediction to be good. As a second point, since $b_i = a_i^*$, both E^f and E^b depend on the a_k and we can compute these coefficients by minimizing the total error $E = E^f + E^b$. The latter method is known as the Modified Covariance (MCOV) and is more robust than the COV method [14].

A minor problem with the MCOV method is that the AR filter used to produce the predicted sequence is not granted to be stable, which is undesirable. This problem is circumvented by an alternative way of computing the coefficients, known as the Burg method [14]. In this method, the coefficients are still computed by minimizing the error E, but are subject to an additional constraint which grants a stable filter. As an additional merit, the minimization can be performed using the Levinson-Durbin recursion, making the Burg method more efficient than the MCOV method. As a drawback, when the sequence is a sum of sinusoids, the Burg method does not produce the coefficients realizing the exact prediction.

IV. Resolution enhancement and EMI suppression

Since the spectrum of Equation (2) is the sum of a set of complex sinusoids plus noise, linear prediction can be used in the frequency domain in order to reliably extrapolate or interpolate the spectrum. This fact is exploited in this Section in order to derive both a super-resolution method and an EMI suppression method.

A. EMI suppression

Consider the received signal of Equation (1). This signal is sampled by the receiver, with a sampling frequency $f_s > B$ and a sampling interval $T_s = 1/f_s$. Assuming that T_f is a multiple of T_s, a sequence of $N = T_f/T_s$ samples is produced. We denote the sampled sequence by $r[n]$ for $n = 1, ..., N$. Moreover, by taking the Discrete Fourier Transform (DFT) of $r[n]$, a sampled version of the signal spectrum of Equation (2) is obtained, denoted by $R[k]$ for $k = 1, ..., N$. As seen from the equation, when the signal is affected by EMI, the spectrum has sinc shaped peaks, centered at the EMI frequencies. The width of the peaks depends on the ratio of the sampling frequency to the system bandwidth and can be approximated as an integer $W > f_s/B$. In order to suppress the EMI, we use the following steps

1. Compute M prediction coefficients from the spectrum.

2. Detect the EMI and mark W samples around each peak.

3. Produce backward and forward predictions for the marked samples.

4. Replace the marked samples with the average of the two predictions.

The method is simple and intuitive. It has a single parameter, namely the prediction order M, which can be set by using simulations. As a comment, note that in the second step we need to detect the EMI: this task is not difficult, since the EMI peaks are normally much higher than the spectrum level, and can be performed using an adaptive threshold detection. A deeper discussion of this point is outside the scope of the paper but can be found in [11], [15].

B. Super-resolution

Linear prediction can be used to enhance range resolution too. Indeed, from Equation (2), we see that the compressed signal spectrum is a sum of complex sinusoids spanning the system's bandwidth B. Then, we can use linear prediction in order to extrapolate the sinusoids beyond the sounder's bandwidth, thereby granting to the system an artificial bandwidth expansion that will sharpen the pulse when the spectrum is transformed back in the time domain. Specifically, we can perform the following steps:

1. Compute M prediction coefficients using the spectrum.

2. Extrapolate K samples to the right (past the N-th sample) by using forward prediction.

3. Extrapolate K samples to the left (before the first sample) by using backward prediction.

Using the latter steps, the effective bandwidth is increased by a factor $B_e = (2K + N)/N$, which will be called the bandwidth expansion factor (BEF). In the time domain, the main lobe of the sinc pulses is narrowed by the same factor. Again the method is simple and intuitive. It has two main parameters, namely the number of coefficients M and the BEF. Suitable settings for these parameters can be investigated by means of simulations.

C. Experiments using simulated data

In order to investigate the performance we carried out experiments using simulated data. In the following we present an example aimed at studying the performance of the super-resolution method when $BEF = 3$ and $M = N/3$. We assume $N = 1800$, $B = 10$ MHz and two layers with a separation of 150 m and complex amplitudes $\alpha_1 = 1$ and $\alpha_2 = 0.5$, which are parameters adequate for a SHARAD frame.

As a first step, we produce an ideal, high resolution spectrum, denoted by $\hat{R}_k$ and having $\hat{N} = 3N$ samples. The spectrum is produced using the discrete version of Equation (2) with two layers, no EMI and no noise. From this spectrum, we extract the N central samples and add white noise according to a given SNR. The resulting sequence is denoted by $R[k]$ and is regarded as the spectrum seen by the sounder. To this spectrum, we apply the super-resolution method and extrapolate it by using $K = N$ (i.e. $BEF = 3$) and $M = N/3$. The resulting super-resolution spectrum has $3N$ samples, and
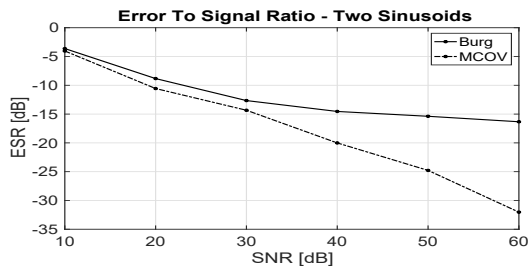
Fig. 2.   ESR for varying SNR for the Burg and the MCOV methods.

Fig. 3.   Full resolution, low resolution and enhanced resolution squared magnitude of a SHARAD frame.

is denoted by $\bar{R}[k]$. In order to evaluate the extrapolation performance, we define a reconstruction error as the difference of the ideal and the extrapolated spectrum, i.e.

$$E[k] = \hat{R}[k] - \bar{R}[k],$$

and compute an Error to Signal Ratio (ESR), given by

$$ESR = \frac{\sum_{k=1}^{K} |E[k]|^2 + \sum_{k=N+K+1}^{N+2K} |E[k]|^2}{\sum_{k=K+1}^{K+N} |\hat{R}[k]|^2}.$$

The ESR is reported in Figure 2, for varying SNR, averaged over 100 noise realizations, when the extrapolation is carried out using the Burg and the MCOV methods. From the Figure we see that, as soon as the SNR is greater than 20 dB, the ESR is lower than -10 dB, indicating that the extrapolation is reliable. As expected, for high SNR, the ESR is lower for the MCOV method, which can perfectly predict the sinusoidal signals, than for the Burg method. As a result the MCOV may be preferable in this SNR regime. On the other hand, when the SNR is low, the two approaches have a similar performance. In this case, the Burg method may be a better choice because it grants a stable filter.

The simulator has been used to investigate the vaules of the algorithm's two main parameters, namely the BEF and the number of coefficients, for a range of practical operating conditions (SNR, number of layers etc.). The full results are reported in [15]. Concerning the BEF, we have observed that, as is intuitive, the ESR increases for increasing BEF. Therefore, the maximum BEF can be obtained by assigning a target ESR. For example, assigning $ESR = -20$ dB, the maximum BEF ranges from 2 to 4 depending on the operating conditions. Concerning the number of coefficents M, by running simulations with varying M, we have observed that the ESR has a minimum, which is mildly dependent on the operating conditions and is usually close to $M \approx N/3$.

D. Experiments using real data

In order to validate our methods we also carried out experiments using real data. An example, similar to the one carried out for simulated data, is described in the following. In the experiment, we start from a real, full resolution SHARAD spectrum, denoted by $\hat{R}[k]$ and having $\hat{N} = 1800$ samples. From this spectrum, we extract the $N = 600$ central samples and obtain a sequence denoted by $R[k]$ for $k = 1,...,N$
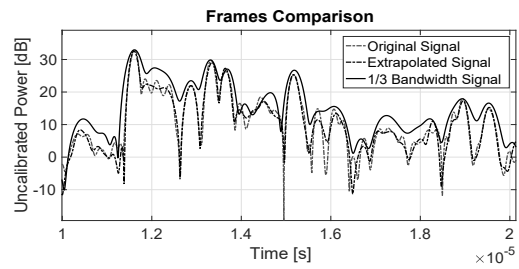
which is a low resolution spectrum. Using the low resolution spectrum, we extrapolated $K = 600$ samples to the left and to the right, using an AR filter with 200 coefficients, in order to produce a super-resolution spectrum $\bar{R}[k]$ which has the same resolution of the original spectrum. The corresponding time domain data, obtained by means of an Inverse DFT (IDFT) of the spectra, are reported in Figure 3. From the figure we see that the super resolved data are very close to the original data, indicating that the approach is indeed accurate. Moreover, we can appreciate resolution improvement by comparing the main lobe of the low-resolution spectrum with those of the two high resolution ones.

V. APPLICATION TO MARSIS DATA

The MARSIS instrument [2] is a low-frequency, nadir-looking, pulse-limited radar sounder using unfocused SAR. The radar operates in four channels between 1.8 and 5.5 MHz by transmitting chirp signals with 1 MHz bandwidth and 250 usec duration. The expected ground penetration is a function of the nature of the crust and can be up to 5 Km. In the ground data processing, the return signal is compressed in order to achieve a range resolution of 150 m in the free space.

The typical MARSIS observation consists of six frames, obtained from three Doppler filters over two center frequencies. Each frame is constituted by 512 complex samples. The data are processed separately for the two center frequencies. Specifically, in the standard processing, a Hanning window is applied to each frame, in order to reduce the side-lobes and prevent the subsurface returns being masked by the first surface reflection. Next, the three frames are summed incoherently, which is an effective way to reduce the speckle noise. On the other hand, in the enhanced processing, we apply the EMI suppression followed by the resolution enhancement with a BEF of 3. In both cases we employ the Burg method and $M = N/3$. Then, the Hanning window is applied to the extrapolated spectrum, in order to reduce the sidelobes. Finally, the three frames are summed incoherently.

As a first example of the results, in Figure 4 we present the squared magnitude of a radargram obtained from the 4 MHz center frequency, covering the North Polar Mars' region, where a two layer structure is clearly seen. Both the standard radargram (top) and the enhanced one (bottom) are presented. Observing the figure we see that the range resolution is clearly
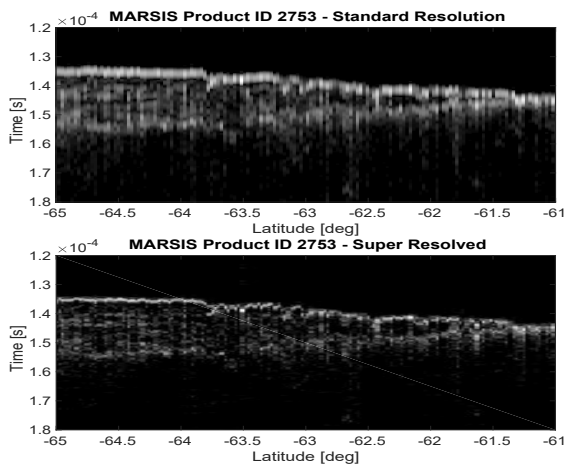
Fig. 4. Standard and enhanced radargrams for a MARSIS observation of the Mars' North pole. Black to white range: 40:80 dB.
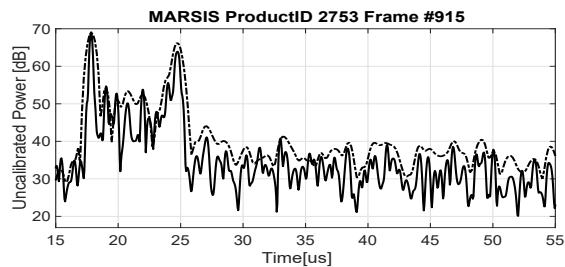

Fig. 5. Squared magnitude of a standard (dotted) and enhanced (continuous) frame of the radargram of Figure 4.

improved. Moreover, the enhanced radargram is less noisy, which is due to the EMI suppression. Both facts are also seen in Figure 5, reporting a single frame of the two radargrams. In particular, we see that the enhanced frame has a narrower lobe and a lower noise level. As a final comment, note that, by inspecting the complex data, we verified that the amplitude and the phase of the surface and subsurface peaks are preserved by the enhancement processing: this is an important aspect, since these two parameters yield information useful for several applications. In Figures 6 we present a second example taken over the South Polar Mars' region, again at 4 MHz. Entirely similar comments apply.

VI. CONCLUSION

We presented a super-resolution method and an EMI suppression method for radar sounders products, both based on linear prediction. The methods grant an enhanced range resolution and a lower noise level in the radargrams. We investigated the methods' performance and parameter settings using both simulated and real data. Finally, we discussed the application to the MARSIS data and presented examples of the results.
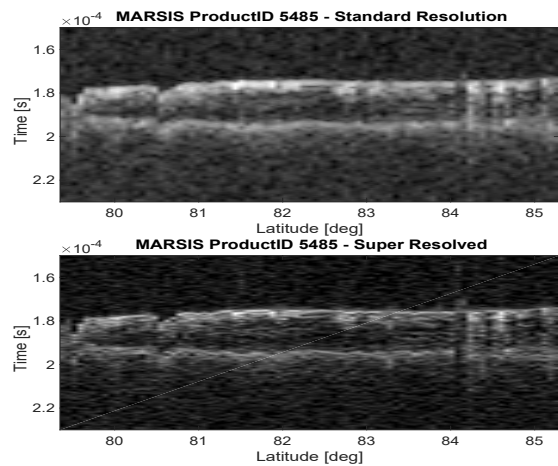

Fig. 6. Standard and enhanced radargrams for a MARSIS observation of the Mars' South pole. Black to white range: 20:70 dB.

REFERENCES

[1] L.J. Procello et al.,"The Apollo Lunar Radar Sounder system", Proc. IEEE, vol. 62, no.6, pp.769-783, June 1974.
[2] G. Picardi et al., "Radar sounding of the subsurface of Mars", Science 310, 1925-1928, November 2005.
[3] R. Seu et al., "SHARAD: the MRO 2005 shallow radar", Planetary Space Sci.,vol. 52,pp.157-166, January 2004.
[4] Kobayashi, T. et al., "Synthetic Aperture Radar processing of Kaguya Lunar Radar Sounder data for Lunar Subsurface Imaging", IEEE Trans. Geosci. Remote Sensing, 50(6), 21612174, June 2012.
[5] L. Bruzzone et al., "RIME: Radar for icy moon exploration", in Proc. IEEE IGARSS, pp. 39073910, July 2013.
[6] A. Eremenko et al., "Europa Clipper spacecraft configuration evolution", 2014 IEEE Aerospace Conference, pp. 1-13, Big Sky, MT, March 1-8, June 2014.
[7] S.B. Bowling, "Linear Prediction and Maximum Entropy Spectral Analysis for Radar Applications", Project Report RMP-122, MIT Lincoln Laboratory, May 1977.
[8] K.M. Cuomo, "A Bandwidth Extrapolation Technique for Improved Range Resolution of Coherent Radar Data', Project Report CJP-60, MIT Lincoln Laboratory, December 1992.
[9] T.G. Moore, "Enhanced Imagery using spectral-estimation-based techniques", Lincoln Lab. J., vol.10, no. 2, pp-171-186, 1997.
[10] M. Mastrogiuseppe et al., "The Bathymetry of a Titan sea", Geophys. Res. Lett., vol. 41, no.5, pp. 1432-1437, February 2014.
[11] M. C. Raguso, M. Mastrogiuseppe, R. Seu, L. Piazzo "Super-Resolution and Interferences Suppression Techniques applied To SHARAD Radar Data", submitted to IEEE Metrology for Aereospace, 2018.
[12] M. Restano, M. Mastrogiuseppe, A. Masdea, G. Picardi, and R. Seu, "Ionosphere Compensation and Stepped Frequency Processing in the MARSIS Experiment", IEEE 3rd Microwaves, Radar and Remote Sensing Symposium, pp. 149-152, Kiev, Ukraine, August 2011.
[13] Daniels D.J., "Ground Penetrating Radar", 2nd ed., London, U.K.:Inst. Eng. Technol., 2007
[14] S. L. Marple, Jr., "Digital Spectral Analysis with Applications", Englewood Cliff, NJ: Prantice Hall, 1987.
[15] M.C.Raguso, "Sounder Data Processing and Techniques for Geophysical Parameters Estimation", PhD Thesis in preparation, DIET Dept., Sapienza University, 2018.